Journal on Materials and its Characterization

Vol: 4(3), September 2025

REST Publisher; ISBN: 2583-6412

Website: http://restpublisher.com/journals/jmc/

DOI: https://doi.org/10.46632/jmc/4/3/2

Biophysical Interaction Specificity of Naringenin Functionalized Silver Nanoparticles with Human Serum Albumin

[1,2]Chinnu V Devan, [1]Surya Sukumaran, [1]Riju K Thomas, [1]Prasanth S, *[1]C Sudarsanakumar

[1]School of Pure and Applied Physics, Mahatma Gandhi University, Kottayam, Kerala, India.

[2]Mahakavi Vennikulam Government Polytechnic College, Pathanamthitta, Kerala, India.

*Corresponding author Email: c.sudarsan.mgu@gmail.com

Abstract: *The natural drug, Naringenin (Nar) based synthesis of drug-functionalized silver nanoparticles (AgNPs), has gained much attention in biomedicine owing to its unique optical and therapeutic properties. The present study deals with the biosynthesis of drug-functionalized AgNPs using Naringenin as a capping agent. Further characterization of Naringenin-AgNPs (Nar-AgNPs) was done by a combination of FTIR, XRD & TEM analysis. The TEM analysis revealed that most of the Nar-AgNPs attained a spherical morphology of around 30 nm. The mode of interaction between Nar-AgNPs with human serum albumin (HSA) was explored using a series of spectroscopic, calorimetric and CD analysis. The thermodynamic kinetics, including the binding energy, binding stoichiometry and thermal variations coupled with the AgNPs-HSA complexation, was also evaluated by ITC. The fluorescence spectroscopic study revealed that the intrinsic fluorescence of HSA was significantly quenched upon the binding of Nar-AgNPs. The minor local conformational alterations attained by the secondary structure of HSA when being complexed with Nar-AgNPs were further explored by CD spectral analysis. The comprehensive and better understanding of Nar-AgNPs interactions with medically significant plasma protein, HSA, threw new light towards drug delivery thereby suggesting its diverse applications in nano medicine.*

Keywords: *Silver nanoparticle, Naringenin, Human serum albumin*

1. INTRODUCTION

Nanotechnology and nano-based therapies are the emerging fields of research focused towards the redefinition and bio-functional evaluation of metallic nanoparticles (NPs) with exclusive optical, magnetic and electrical properties [1,2]. These remarkable optical properties and homogeneity of the metal-functionalized NPs had gained renovation with potential applications in diverse areas of nonlinear optical devices, biotechnology, healthcare, biomedicine, electronics and targeted drug delivery [3-5]. Silver, a unique material whose plasmon resonance can be tuned to any wavelength in the visible spectrum, has long been renowned for its biocidal/ antimicrobial effect even against multidrug-resistant microorganisms [6,7]. Hence, among the diverse metal functionalized NPs, the silver nanoparticles (AgNPs) represent one of the most explored and promising candidates, which showed effective interaction with light than a particle of identical dimension with several known organic or inorganic chromophores [8]. Thus, the AgNPs are being widely exploited as drug carriers in diverse fields of biomedicine, infertility management, cancer treatment and diagnosis due to their shape adjustability, high-density surface ligand attachment and trans membrane delivery potential [9-12]. Nowadays, the biologically inspired green synthesis of natural drug functionalized metal NPs has been suggested as a non-toxic and eco-friendly alternative replacing the hazardous conventional physicochemical methods. In such eco-friendly synthesis, the functionalizing agents of metal NPs are replaced by bio-active plant extracts, enzymes, natural and synthetic drugs, polymers and vitamins [13,14]. The capping agents involved in green synthesis are the core player offering solubility, shape, reactivity and stability to the NPs. Thus plant-mediated synthesis of AgNPs gained immense popularity due to its execution-simplicity and its

remarkable applications as nano" carriers to overcome the biological barriers by specific drug targeting to the site of action [15, 16].

Phytochemicals (PC) like alkaloids, flavonoids and terpenoids are plant-based biologically active compounds considered to be beneficial for human health. PC also possesses polyhydroxy groups, which are responsible for its free radical scavenging property by playing a central role in reducing metal ions into NPs [17]. Naringenin (Nar) is one such flavanone found in a glycol form, widely used in traditional Chinese medicine formulations offering rich sources like grapes, herbs and other citrus fruits [18]. The Nar is chemically known as 5,7-Dihydroxy-2-(-4-hydroxyphenyl) chroman-4-one existing in nature as both a glycol form (Naringenin) and in its glycosidic type (naringinin). Recently due to its extensive pharmacological effects like anti-inflammatory, antitumor, antifibrogenic, antihyperglycemic and antihyperlipidemic properties, Nar has gained more attention [19-21]. Nar is a hydrophobic crystalline compound with deprived oral bioavailability, thereby restricting its therapeutic index. To this point of view, a great deal of effort has been employed to improve the drug efficacy, i.e. bioavailability and solubility, by capping the natural drug, Nar, into its nanoparticle form [22]. The synthesis and characterization of flavonoids based AgNPs from hesperidin, naringin, and diosmin had already been reported with efficient bactericidal and cytotoxicity effects against human promyelocytic leukemic (HL-60) cell lines [23]. In this study, Nar was used for the green synthesis of AgNPs, and they were further characterized and utilized for the interaction studies with HSA might have a new approach towards pharmacokinetics.

The NPs can interact with biomolecules such as proteins, lipids and nucleic acids due to their surface properties. The dynamic interaction of NPs with proteins in a biological medium gives rise to protein corona formation and might induce conformational changes leading to overall bio reactivity [24]. The fate of NPs bound drugs, when compared with the conventional forms, have an extended half-life, longer circulation times and can even load a high concentration of a potent drug to the target site of action [25-27]. The size and surface characteristics alteration improves its desired delivery property by reducing its toxicity and acquiring biocompatibility [28]. The sensible utility of NPs in biomedicine by unlocking the mystery requires the entire dataset concerning the binding affinity and alteration in the protein conformation upon NPs binding, which in turn reflects in the protein stability. HSA is the most stable, abundant and soluble plasma protein involved in the binding and transport of endogenous substances within the human circulatory system [29]. Towards this goal, we selected HSA for investigating the interaction studies with Nar-Ag NPs as a model system. HSA is one of the extensively studied transport globular proteins showing structural homology with bovine serum albumin [36]. It is of molecular weight 66kDa with 585 amino acids forming a polypeptide chain stabilized by 17 disulfide bridges. It is a multifunctional, non-glycosylated; negatively charged plasma protein synthesized in the liver and might nonspecifically contribute to colloid osmotic pressure maintenance. The tertiary structure of HSA (**Fig. 1**), composed of three alpha-helical domains (I, II, III) assembled to form a heart-shaped molecule, has a single tryptophan residue (Trp-214), 18 tyrosines and six methionine [37]. The single Trp-214 residue located in site 1 of HSA has been used extensively as a fluorescent reporter group for measuring the affinity of ligand binding and conformational studies. The main ligand binding sites of HSA are located in the hydrophobic pockets II A and III A, and out of these two pockets, site III A exhibit higher binding affinity [38, 39]. An extensive study regarding the interaction of HSA to various drug moieties and their alteration in the binding ability, intern reflected in pharmacokinetics reversibly, has been studied to a great extent [40, 41].

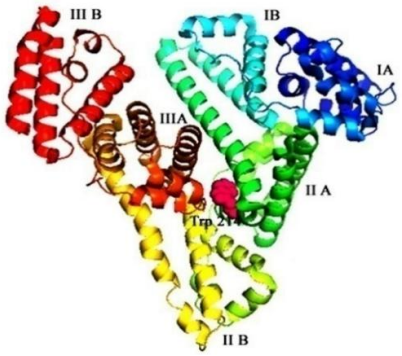

FIGURRE 1. Alpha helical domains of HSA (PDB ID: 1H9Z) with highlighted Trp 214 residue.

A handful of literature is available on the interaction strategy of Ag, CdS, Se and Au metal NPs with HSA [30-33]. More many researchers also reported on the binding strategy of metal oxide NPs like TiO_2 and ZnO [34,35] with HSA. However, to our knowledge synthesis, characterization and binding mechanism of Nar-AgNPs with HSA are not accessible in the literature so far. The present work focuses on the concept that HSA is the drug carrier protein model for investigating the binding mechanism of Nar-AgNPs to validate its biocompatibility for promising drug research. Targeting Nar-AgNPs-HSA interaction is far more challenging, but we systematically investigated the interaction of Naringenin-capped NPs with HSA by a series of conventional spectroscopic and calorimetric methods. The quenching of the intrinsic tryptophan fluorescence of HSA and the thermodynamic parameters associated with the interaction was determined by fluorescent spectroscopy and ITC. The conformational changes that evolved in the secondary structure of HSA upon Nar-AgNPs interaction were further investigated by CD spectroscopy. In this context, the presented work may be considered a logical research strategy to understand how the Nar-Ag NPs behave within the biological systems.

2. EXPERIMENTAL SECTION

2.1. Materials

The Naringenin and Human serum albumin (HSA) were purchased from Sigma Aldrich., India. Sodium phosphate monobasic and dibasic for Phosphate buffer (pH-7) preparation was purchased from Merck. The silver nitrate and ethanol were procured from Central drug house (CDH). All other chemicals used for the synthesis were of analytical grade and used devoid of further purification.

2.2. Synthesis of Naringenin capped Silver nanoparticles

For the simple one-pot synthesis of Nar-Ag NPs, 1 mM of silver nitrate ($AgNO_3$) and (1 mM) Naringenin were used as stock solutions. About 14mg of Nar was dissolved in 5ml ethanol as they are sparingly soluble in water, allowed to stir for 30 minutes and finally made up to 10 mL by adding distilled water. About 10 mL of $AgNO_3$ solution was introduced into 10 mL of the above Nar solution by maintaining a 1:1 ratio. Thereafter constant stirring at room temperature for 20 minutes by slightly increasing the pH using 0.01 M NaOH (**Fig. 2**). The formation of Ag NPs was observed by monitoring the colour change to yellowish brown, indicating the formation of Nar-Ag NPs.

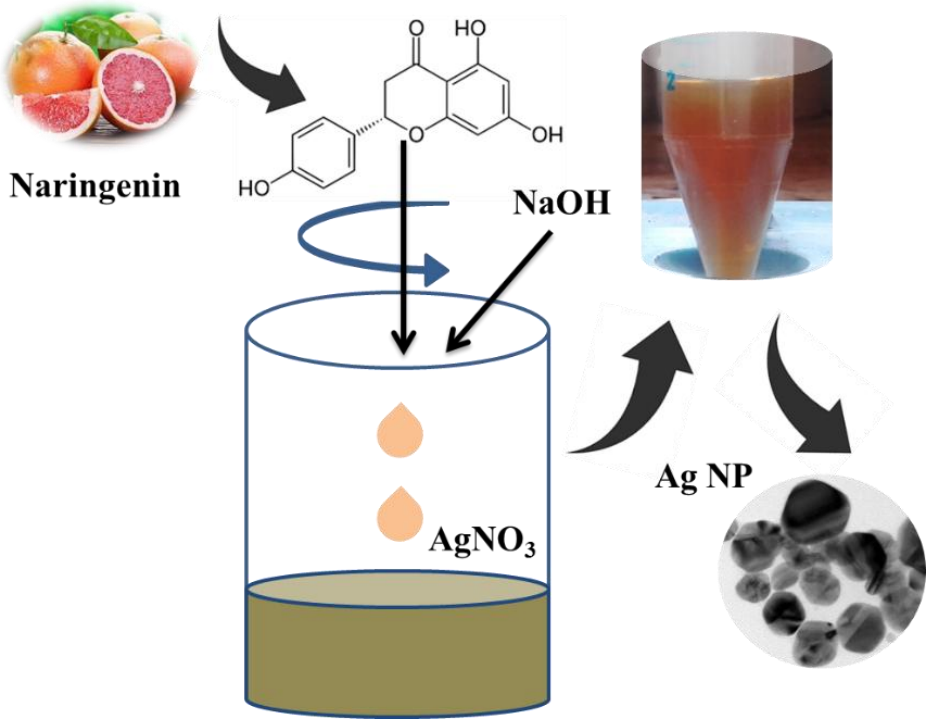

FIGURRE 2. Schematic representation of the synthesis of Naringenin capped Ag NPs.

The stock solution of HSA (0.6mM) was prepared by dissolving 387 mg in 10ml phosphate buffer (pH-7) kept at 4 °C and used for further interaction studies. Nar-Ag NPs at different concentrations ranging from 3- 13 µM were permissible to interact with a constant concentration of HSA (12µM) at room temperature.

2.3. Biophysical Characterization Techniques

The absorption spectrum of synthesized Nar-Ag NPs was recorded using a Shimadzu-2401 UV-visible spectrophotometer in the wavelength range of 200-600 nm. For XRD analysis, the Nar-Ag NPs solution was placed in coverslips and dried at 60°C in a hot air oven. The dried samples were scrapped out into fine powder and analyzed in an X-ray diffractometer. The diffraction spectrum was recorded by PANalytical X-ray diffractometer with CuK α radiation (λ= 1.5406 Å) in the 2 θ range of 10-90°. The morphology, microstructure and distribution of the Ag NPs were characterized by using high-resolution transmission electron microscopy (HRTEM) (JEOL JEM 2100 with LaB6 filament) with an operating voltage of 200 kV. The presence of Naringenin on the surface of Ag NPs was confirmed from Fourier transform infrared (FTIR) spectroscopy and was obtained by using Shimadzu Model: IR Prestige 21, with a ZnSe ATR crystal (Pike technologies) spectrometer at room temperature in the wavelength range of 4000-500 cm-1. The fluorescence spectrum of the HSA-Nar-Ag NPs complex was measured using Fluoromax-4 Spectrophotometer with a spectral slit width of 3 nm and an excitation wavelength of 290 nm. The extent and rate of structural changes intertwining the interaction of Nar-Ag NPs on the secondary structure of HSA were determined by using far-UV CD spectroscopy recorded in the range of 190-260 nm. The CD spectrum was obtained from a Jasco-815 spectropolarimeter with a scan rate of 200nm/min using a quartz cuvette of 1 cm path length and 10 mm cell length.

Interaction studies of Nar-Ag NPs with HSA by ITC

The ITC is becoming a sensible method for determining intermolecular interactions by means of thermodynamic parameters. The calorimetric titrations were performed by using VP-ITC isothermal titration calorimeter from Micro-cal (Northampton, MA, USA) at 298.15 K to characterize the thermodynamic parameters of Nar-Ag NPs-HSA interaction. About 0.01 mM HSA and 0.2 mM Nar-Ag NPs solutions were prepared in a phosphate buffer of pH-7 for the binding experiments in order to validate the interaction kinetics. The samples were degassed prior to loading to prevent the interference of air bubbles. A total of 29 injections were made with a stirring speed of 307

rpm. A time interval of 180 seconds was also set between injections to allow the consecutive peaks of each injection to return to the baseline. The volume of the first injection was set as 3µL to avoid inaccuracy. The final data obtained after the injection, i.e., the amount of heat liberated per injection as a function of the molar ratio of Nar-Ag NPs to HSA, were fitted by a nonlinear least square method using ORIGIN software.

3. RESULTS AND DISCUSSION

3.1 Characterization of Nar-Ag NPs

The formation of Nar-Ag NPs is further confirmed through P-XRD and UV-Vis analysis. **Figure 3a** shows the PXRD pattern of as-prepared Ag nanoparticles through the green synthesis method. The distinct diffraction peaks at 2 values of 37.80°,44.17°,64.24° and 77.17° corresponding to the (111), (200), (220) and (311) planes of the face-centred cubic structure of silver nanoparticles (JCPDS 893722)[42]. The absorption spectrum of Nar-Ag NPs exhibited a broad surface plasmon resonance (SPR) peak in the visible range centred at 450 nm (**Fig. 3b**). The SPR absorption depends on the size and shape of the metal NPs, dielectric constant of the metal and surrounding medium [43]. The SPR peak is broadened due to the polydispersed NPs.The inset of **Figure 3b** shows the absorption spectra of Nar-Ag NPs after 30 days, and it confirms the stability of the green synthesized sample after ageing.

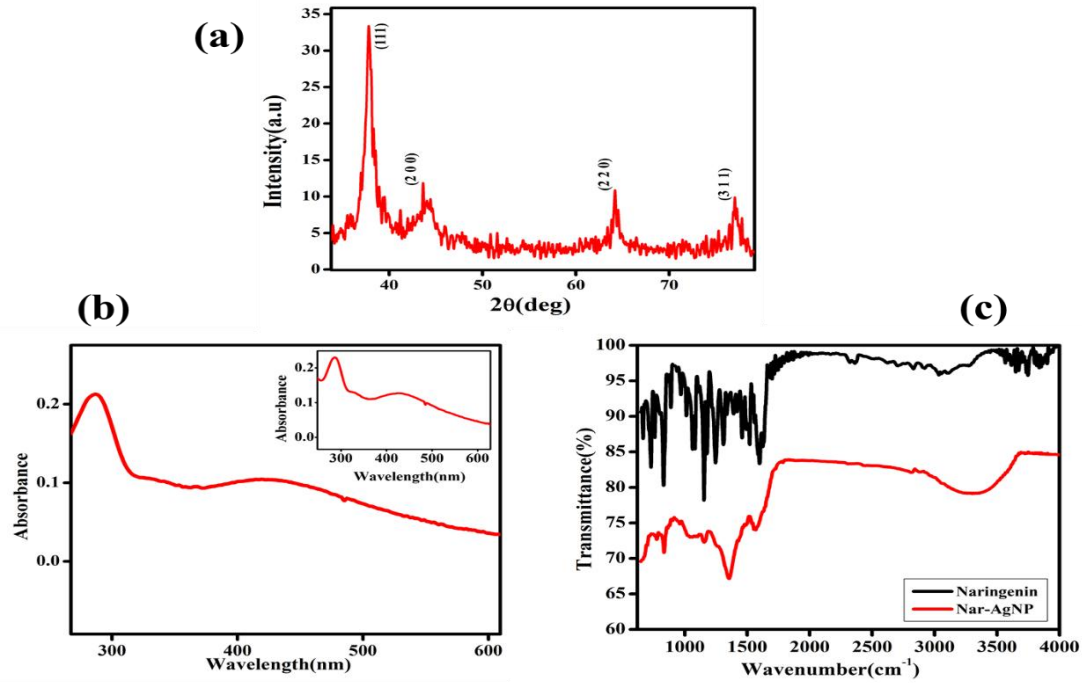

FIGURRE 3. (a). UV-Vis absorption spectrum of Nar-Ag NPs. The inset figure shows the absorption spectra of Nar-Ag NPs after 30 days.**Fig.3 (b)** XRD spectrum of Nar-Ag NPs. **Fig. 3 (c)** FTIR spectrum of Nar and Nar-Ag NPs.

The flavonoid compounds like Nar, which have lower redox potential and a higher number of hydroxyl groups, exhibited efficient electron transfer and are reliable in making more Ag NPs [44]. The effective capping of Nar on the surface of Ag NPs was confirmed from the FTIR spectrum (**Fig. 3c**). Observable shifts are corresponding to the absorption of infrared waves by different functional groups at 3040cm^{-1}, 1604cm^{-1}, 1323cm^{-1}, 1152cm^{-1} and 829cm^{-1}. The 3000-3500 cm^{-1} peak corresponds to O-H group vibrations of Nar, and the C-H plane bending vibrations is observed at 1323 cm^{-1}. The peak at 1604 cm^{-1} signifies C-C stretching vibrations, 1152cm^{-1} and 829cm^{-1}, attributed to C-O stretching vibrations. The increased intensity of the hydroxyl group may be due to the binding of ions to the -OH group [32,45, 46].

In the FTIR spectra of Nar-Ag NPs, there is a sudden dip at the range of 3000-3500cm^{-1}; the broad and intense peak confirmed the capping of Nar on the surface of AgNPs.

The HRTEM images revealed that most of the particles are spherical, some in hexagonal shape with an average particle size of 30 nm (**Fig. 4a &b**). **Fig.4c** shows HRTEM images of Nar-Ag NPs with the d-spacing of 0.23 nm and 0.15 nm, corresponding to the planes (111) and (220), respectively. The selected area electron diffraction (SAED) pattern (**Fig.4d**) showed characteristic diffraction rings corresponding to the face-centered cubic (FCC) structure of Ag NPs (111, 220, 311). The HRTEM image and SAED pattern are consistent with the XRD spectrum, confirming the FCC crystalline structure of the synthesized Nar-Ag NPs.

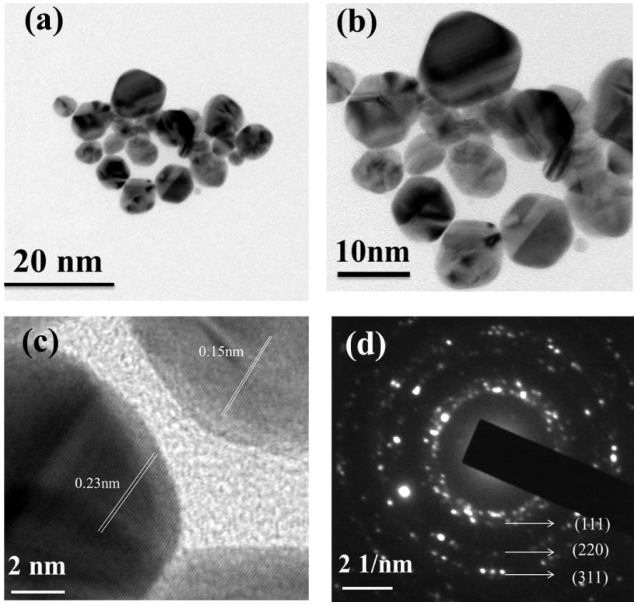

FIGURRE 4. (a) & (b) TEM Images**, (c)** HRTEM image and **(d)** SAED pattern of Nar-Ag NPs.

3.2. Biophysical Characterization of HSA- Nar-Ag NPs Complex

3.2.1. Absorption studies of HSA -Nar-Ag NPs.

The UV-Visible absorbance spectra of the native HSA and HSA conjugated with varying concentrations of Nar-Ag NPs were analyzed and depicted in Fig. 5(a). The UV region of the spectra exhibited a strong band at 278nm, which originates from the aromatic residues tryptophan, tyrosine and the disulfide bonds in the proteins [47]. With the addition of Nar-Ag NPs, the absorbance of HSA increases gradually without any shifts in the peak position and indicates a ground state complex formation between HSA and Nar-Ag NPs.

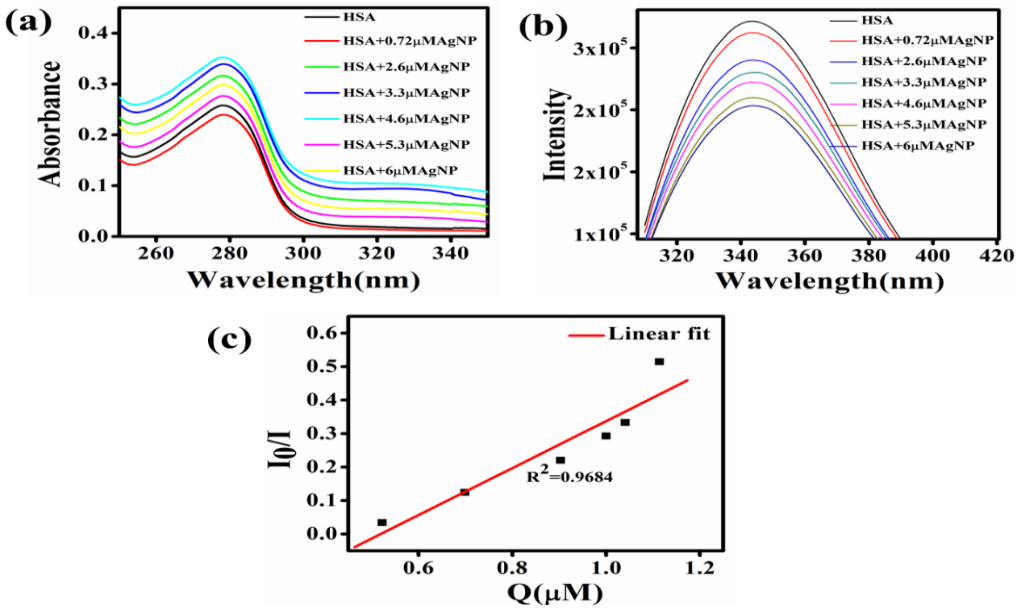

FIGURRE 5. (a). The Absorption spectra of HSA with various concentrations of Nar-AgNPs show a gradual increase in the absorbance of HSA upon increasing the concentration of Nar-AgNPs. **(b)** shows the fluorescence spectra of HSA with various concentrations of Nar-AgNPs and fluorescence intensity of HSA falls consistently with increasing concentration of Nar-AgNPs. **(c)**The Stern-Volmer plot between I_0/and [Q].

3.3. Fluorescence quenching studies of HSA and HSA complexed with Nar-Ag NPs

The fluorescence quenching study is an accurate tool to gain more precise information regarding the binding of Nar-Ag NPs to HSA. Fig.5 (b) shows the fluorescence spectra of HSA and HSA-conjugated Nar-Ag NPs. HSA offers a strong emission peak around 345 nm with an excitation of 290 nm. The tryptophan residue (Trp-214) in the subdomain II A is the major contributor to HSA fluorescence. Tryptophan fluorescence is highly sensitive to changes in the microenvironment [32]. From the figure, it is clear that, on the addition of different (3-13 Mm) Nar-Ag NPs, the fluorescence intensity of HSA quenches. The quenching of fluorescence indicates some strong interactions between HSA and NPs, and the intensity variation is due to the binding of Ag NPs to HSA at a location near the Trp214 residue. The spectral change provides clear-cut evidence towards forming a ground state complex [49]. The quenching can be analyzed by the Stern-Volmer equation[32],

$$\mathbf{I_0/I = 1 + KSV[Q]}$$

WhereI_0 and I indicate the fluorescence intensities of HSA in the presence and absence of Nar-Ag NPs. **KSV** is the Stern-Volmer constant which means the sensitivity of a fluorophore to the quencher, and **[Q]** is the particular concentration of Nar-Ag NPs. The plot of **I_0/I** versus varying concentrations of silver Ag NPs is shown in **Fig. 5 (c).** The value of **KSV** can be calculated from the slope of the straight line and is found to be **0.037×106 M^{-1}**. The Stern-Volmer constant, **KSV** and biomolecular quenching rate constant, **K_q**, are correlated by the equation.

$$\mathbf{KSV = Kq\tau_0}$$

K_q is calculated as **5.6×1012 $M^{-1}S^{-1}$.τ_0** is the lifetime of HSA in the absence of quencher (2.89×10-7 s).

HSA consists of three homologous alpha-helical domains (domains I, II, and III). Each domain comprises two subdomains (A and B) and has multiple ligand-binding sites localized in these two subdomains (**Fig. 1**). The single Trp-214 located in subdomain IIA has been used extensively as a fluorescent reporter for ligand binding and conformational studies. The overall fluorescence of HSA is contributed by amino acid residues tryptophan, tyrosine, and phenylalanine; among them, tryptophan (Trp-214) is the major contributor, but the other two express less contribution owing to their very low quantum yield [32,50]. Because of the high sensitivity of tryptophan emission

to the local environment in HSA, it is used to investigate the binding mode of drug moieties. The emission spectra show that the tryptophan fluorescence is drastically quenched in the presence of Nar-Ag NPs. The repeated addition of varying concentrations of Nar-Ag NPs did not shift the peak maximum (345 nm), indicating minor alterations in the structure of HSA. Therefore, it is logical to conclude from the observed fluorescence quenching that the possible binding sites of Nar-Ag NP are in the vicinity of the Trp-214 microenvironment of HSA (**Fig. 6**).

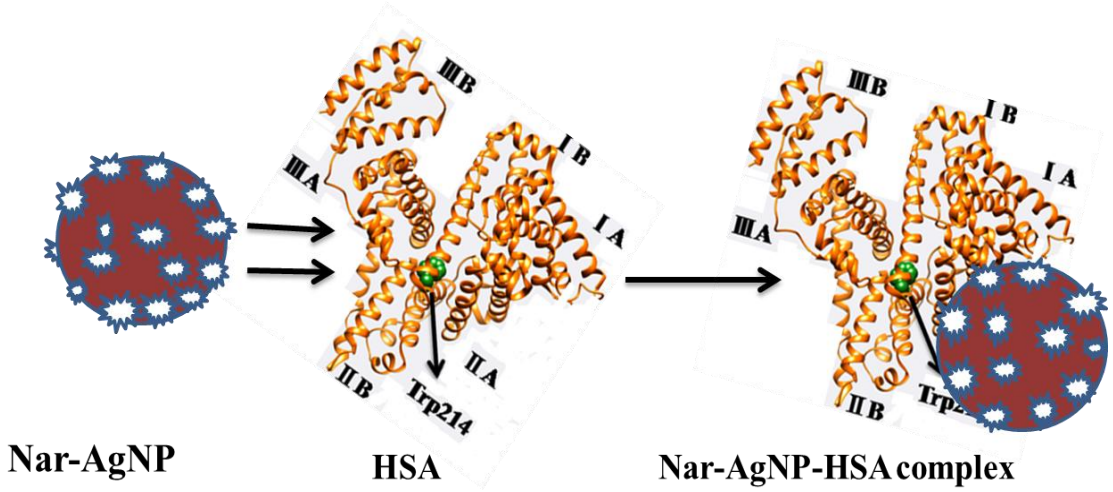

FIGURRE 6. Schematic representation of the interaction between Nar-Ag NP with HSA.

3.4. The Detection of Binding constant and number of binding sites in HSA for Nar-Ag NPs.

The fluorescence quenching data also deduce information about the equilibrium binding constant (K) and the number of binding sites (n)in HSA- Nar-Ag NPs conjugate by using the equation[32,51].

$$\log I_0\text{-}I/I\ [2] = \log K + n \log[Q]$$

Fig.7 illustrates the **log I_0-I/I** plot against **log [Q].** The values of **K** and **n** can be calculated from the straight-line equation. The Y-intercept and slope of the line give K and n, respectively; the resultant values are 2.2 ×106 M^{-1} and 1.72.

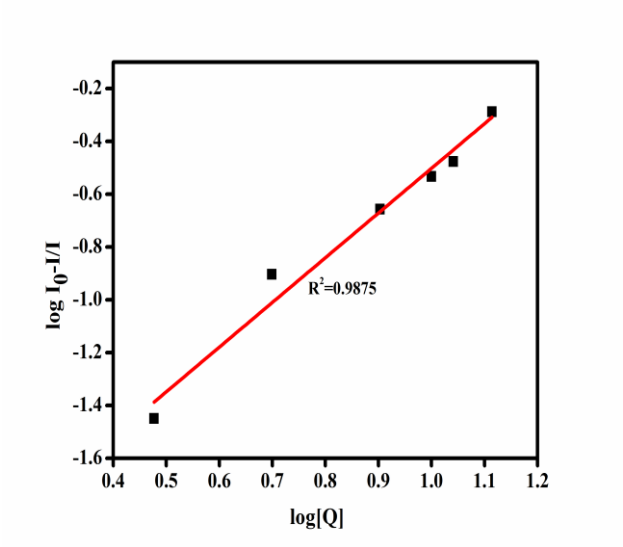

FIGURRE 7. The plot of logI0-I/I versus log [Q].

3.5. Fluorescence resonance energy transfer to the Nar-Ag NPs and distance calculation

Forster resonance energy transfer (FRET) efficiently determines the distance between Nar-Ag NPs and HSA protein. In the FRET mechanism, a donor fluorophore in an excited state may transfer its excitation energy to a nearby acceptor chromophore in a non-radioactive approach through dipole-dipole interaction [52, 53, 32]. FRET can occur only when there is a spectral overlap between the emission spectrum of the donor and the absorption spectrum of the acceptor with a separating distance, linking the donor and the acceptor, of within 2-8 nm. The efficiency of the FRET process (EFRET) depends on the inverse sixth power of the distance between the donor and acceptor pair(r) can be expressed as [49].

$$E_{FRET} = \frac{R_0^6}{R_0^6 + r^6} = 1 - \frac{I}{I_0} \qquad [3]$$

Where I and I_0 are the fluorescence intensities of the donor in the presence and absence of the acceptor, R_0 is the critical distance when the transfer efficiency is 50%, and the distance between the donor and acceptor, r, can be calculated using the equation [32].

$$R_0^6 = 8.8 \times 10^{-25} k^2 N^{-4} \phi J \qquad [4]$$

Where k^2 is the spatial orientation factor of the dipole, N is the refractive index of the medium,Φ is the quantum yield of the donor, and J is the overlap integral of the fluorescent emission spectrum and is estimated by [54].

$$J = \frac{\Sigma F(\lambda) \in (\lambda) \lambda^4}{\Sigma F(\lambda) \Delta\lambda}$$

Where F (λ) and are the fluorescence intensity of the donor and molar absorptivity of the acceptor, respectively.

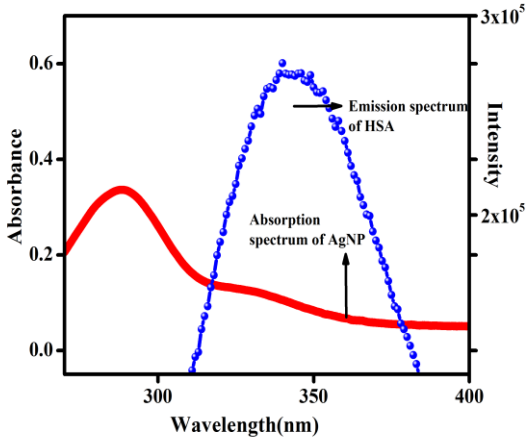

FIGURRE 8. The spectral overlap of the absorption spectrum of HSA and the emission spectrum of Ag NPs.

Fig.8 illustrates the spectral overlap of the absorption spectrum of Nar-Ag NPs with the fluorescence emission spectrum of HSA. By using the values of energy transfer efficiency, J= 1.33×10-16 cm^3 L Mol-1, k^2=2/3, N=1.36 and Φ=0.14 and by using these values, R_0 and r can be calculated. The obtained values are R_0=1.21 nm and r=2.12 nm. Therefore, the binding distance, r, between the Trp donor of HSA and bound Nar-Ag NPs was obtained as 2.12 nm. It reveals that Ag NPs are situated in close proximity to the Trp 214. These distances are consistent with the

reported results and were found to be 2.12 nm indicating a higher probability of energy transfer between the Trp residue and the Ag NPs [32].

3.6 Thermodynamic kinetics by Isothermal titration calorimetric Assay

The thermodynamic interaction kinetics associated with binding Nar-Ag NPs with HAS can be interpreted through ITC. The thermal change was monitored by titrating Nar-Ag NPs sequentially into a solution of HSA, and the mode of interaction was found to be exothermic [32]. The **binding constant (K), change in enthalpy (ΔH), change in entropy (ΔS),** and the **change in Gibbs free energy (ΔG)** was calculated from the equation **ΔG = ΔH-TΔS** and shown in Table 1. The data of the ITC profile (**Fig. 9**) fit into the multiple binding site model giving a binding stoichiometry of n = 3 [32]. The rectangular points in the raw exothermic ITC curve represent the experimental injection heats, and the solid line denotes the calculated fit of the data by a nonlinear least square method [55]. The sign and magnitude of the thermodynamic parameters of Nar-Ag NPs binding to HSA deduced from ITC justified the formation of the HSA-Nar-Ag NPs binary complex suggesting favourable hydrophobic, electrostatic and hydrogen bonding interactions[56].

The Nar-Ag NPs have shown a significantly strong binding affinity with HSA exhibiting an average ΔG of 6.4 kcal mol−1. At the same time, the -ve ΔS (**Table.1**) values of the multiple binding sites on HSA indicate the lower entropy. It was assumed that the probability of hydrogen bond formation is very high in entropically driven reactions. Hence the reaction is entropy driven, and the system is ordered. **Table.1** illustrates that here the mechanism of binding is exothermic and via hydrogen bonding interactions insisting ΔG, ΔH and ΔS are negative [57,32] and is in good agreement in terms of K and N values of fluorescence quenching data, respectively.

TABLE 1. Binding and thermodynamic parameters of the HSA-AgNP system

Temperature (K)	K (M^{-1})	ΔH (cal/mol)	-TΔS	ΔG (Kcal/mol)	n
298.15	1.8×10^{5}	-1.406×10^{4}	7660	-6.4	3

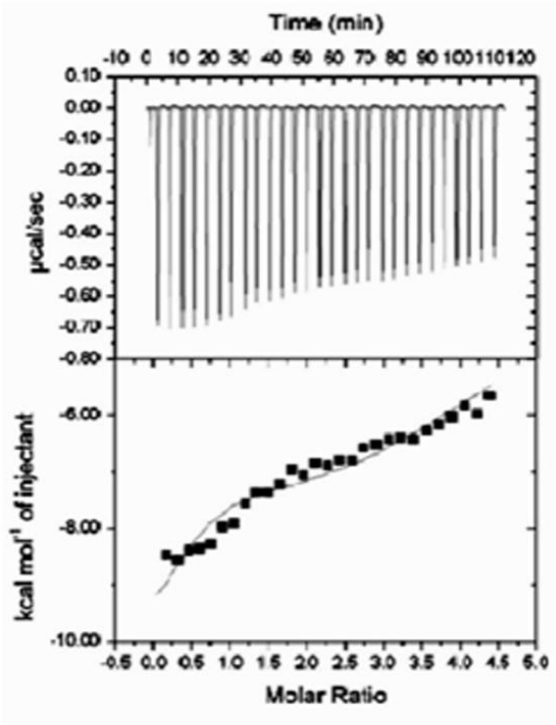

FIGURRE 9. Isothermal titration calorimetric analysis of Nar-Ag NPs (0.01 mM) with HSA (0.2 mM). The curve represents the energy released during the titration as a function of the compound added. Raw thermal power signal(top) and plot of integrated heat versus Ag NPs/protein molar ratio (bottom).

3.7. Circular Dichroism (CD) Spectroscopy

The CD is a reliable technique for evaluating the secondary structure of HSA in solution and can also estimate the changes in the conformation and the folding pattern of HSA upon binding with Nar-Ag NPs. The wavelength-dependent differences in the absorption of left-handed and right-handed circularly polarized light by optically active molecules like HAS [58]. The CD spectra of HSA were recorded in the presence and absence of Nar-Ag NPs (**Fig. 10**). The CD spectra showed two significant firm negative peaks representing the typical distinctive conformation of the α helical proteins at 208 nm and 222 nm. The 208 nm band arose due to theπ-π* transition of the α helix, and the peak at 222 nm is ascribed to the n- π* change for both α- helical and unordered structures. The band at 222 nm is incorporated with the hydrogen bonding nature of α helices and is relatively independent of their length [59]. On the addition of Nar-Ag NPs to HSA, there is a clear decrease in ellipticity due to the binding of Nar-Ag NPs with the HSA, indicating a descent in α helical content. The percentage of α helicity of native HSA and HSA conjugated with varying concentrations of Ag NPs can be estimated from the mean molar residual ellipticity (MRE) [60,61].

$$\textbf{α-helix (\%)} = \frac{\mathbf{MRE_{222} - 3000}}{\mathbf{-36000 - 3000}}$$

MRE designates the direct quantitative measure of the loss of α helical content of a protein. MRE_{222} is the observed value at 222 nm in degree cm2 mol^{-1}, which can be calculated by applying the previously reported equation [62].

$$\mathbf{MRE_{HSA}} = \frac{\boldsymbol{observed\ CD(mdeg)}}{\mathbf{10}\boldsymbol{nCl}}$$

Where n is the number of amino acid residues of HSA (585), C is the molar concentration and (cm) is the path length consecutively. In these characteristic HSA-Nar-Ag NP interactions, the unfolding of HSA increases the concentration of Nar-Ag NPs reflected in the percentage variations in α helical content (62% of pure HSA to 54%) and are scheduled in **Table 2**. A minor conformational change of ~8% is due to partial unfolding and slightly distorted structural integrity induced by the Nar-Ag NPs coupled interaction with HSA.

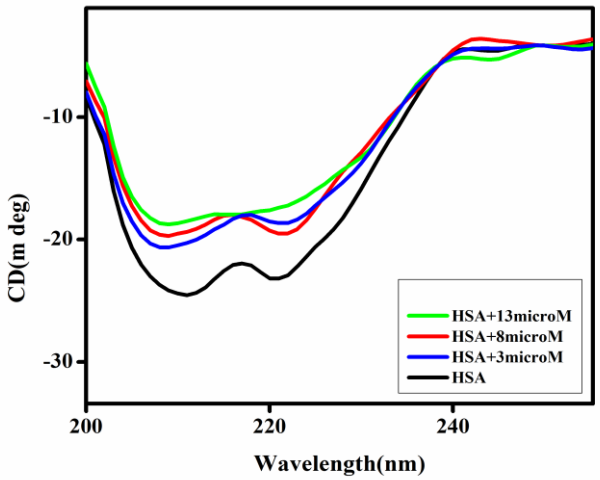

FIGURRE 10. CD spectra of HSA and HSA with various concentrations of Ag NPs.

TABLE 2.The percentage of α helicity on the addition of various concentrations of AgNP

System	α-helix (%)
HSA	62
HSA+3μMAgNP	59
HSA+8μMAgNP	56
HSA+13μMAgNP	54

4. CONCLUSION

Herein, we have explored the interactions study of HSA and Nar-Ag NPs using various spectroscopic and calorimetric techniques. From the XRD and TEM analysis, the average particle size of Nar-Ag NPs was obtained < 30 nm. The absorption and fluorescence quenching studies reveal a ground state complex formation between HSA and Nar-Ag NPs. The nature and energetics of the interaction by ITC exhibited an exothermic binding mode for Nar-Ag NPs, and the exchange was generally through hydrogen bonding. The high energy transfer possibility between the fluorophore (Trp-214) of HSA and the Nar-Ag NPs was estimated from FRET analysis. From FRET analysis and the fluorescence quenching analysis, it is clear that Ag NPs bound near the vicinity of Trp-214 residue. CD spectrometry explores the minimal modification of the secondary structure of HSA associated with the complexation. The present study shed light on the applications of natural drug-functionalized Ag NPs in the field of drug delivery, therapeutics and pharmacokinetics.

Acknowledgements: The author Surya thanks SERB National post-doctoral Fellowship, and Prasanth and Riju thank UGC for BSR-RFSMS fellowships. We also express gratitude to Dr M. Haridas, Inter-University Centre for Bioscience, Kannur University, for providing access to ITC.

REFERENCES

[1]. Duncan, T.V.: Applications of nanotechnology in food packaging and food safety: Barrier materials, antimicrobials and sensors. J. Colloid Interface Sci, 363, 1–24 (2011). https://doi.org/10/1016/j.jcis/2011.07.017
[2]. McEuen, P.L.: Nanotechnology Carbon-based electronics. Nature, 393, 15-17 (1998). https://doi/10.1038/29874.
[3]. Ramos, A.P., Cruz, M.A.E., Tovani, C.B., Ciancaglini, P.:Biomedical applications of nanotechnology. Biophys Rev, 9, 79–89(2017).https://doi.org/10.1007/s12551-016-0246-2
[4]. Nel, A.E., Maedler, L., Velegol, D., Xia, T., Hoek, E.M.V., Somasundaran, P. et al.: Understanding Biophysicochemical Interactions at the nano-bioInterface. Nat. Mater, 8, 543−557 (2009). https://doi/10/1038/nmat2442
[5]. Lal, S., Clare, S.E., Halas, N.J.:Nanoshell-enabled photothermal, cancer therapy: impending clinical impact. Acc. Chem. Res, 41, 1842−1851 (2008). https://doi/10.1021/ar800150g
[6]. Hussain, J.I., Kumar, S., Hashmi, A.A., Khan, Z.: Silver nanoparticles: preparation, characterization, and kinetics. Adv. Mat. Lett, 2, 188-194 (2011). https://doi/10.5185/amlett.2011.1206
[7]. Ravindran, A., Singh, A., Raichur, A.M., Chandrasekaran, N., Mukherje, A.: Studies on interaction of colloidal Ag nanoparticles with bovine serum albumin (BSA). Colloids Surf. B, 76, 32–37 (2010). https://doi.org/10.1016/j.colsurfb2009.10.005
[8]. Evanoff, D.D., Chumanov, G.: Size-controlled synthesis of nanoparticles. 2. Measurement of extinction, scattering, and absorption cross sections. J. Phys. Chem. B 108 13957-13962 (2004). https://doi/10.1021/jp0475640
[9]. Kuppusamy, P., Yusoff, M.M., Maniam, G.P., Govindan, N.: Biosynthesis of metallic nanoparticles using plant derivatives and their new avenues in pharmacological applications – An updated report. SPJ 24 473–484 (2016). https://doi.org/10.1016/j.jsps.2014.11.013
[10]. Raj, D.R., Prasanth, S., Vineeshkumar, T.V., Sudarsanakumar C.: Surface Plasmon resonance based fiber optic dopamine sensor using green synthesized silver nanoparticles. Sens. Actuator B-Chem, 224, 600-606 (2016). https://doi.org/10.1016/j.snb.2015.10.106
[11]. Bhattacharya, R., Mukherjee, P.: Biological properties of "naked" metal nanoparticles. Adv. Drug Deliv. Rev, 60, 1289-12306 (2008). https://doi/10.1016/j.addr.2008.03.013
[12]. Wu, Q., Cao, H., Luan, Q., Zhang, J., Wang Z., et al.: Biomolecule-assisted synthesis of water-soluble silver nanoparticles and their biomedical applications. Inorg. Chem 47 5882-5888 (2008). https://doi/10.1021/ic8002228
[13]. Jun Ding,Guilin Chen,Guofang Chen, Mingquan Guo, One-Pot Synthesis of Epirubicin Capped Silver Nanoparticles and Their Anticancer Activity against Hep G2 Cells, *Pharmaceutics* 2019, *11*, 123; doi:10.3390/pharmaceutics11030123.
[14]. Khan Behlol Ayaz Ahmed, Santanu Kar Mahapatra, Mamilla R. Charan Raja, Shankar Subramanian, Megarajan Sengan, Narendran Rajendran, Sandeep Kumar Das, Kuntal Haldar,Somenath Roy, Aravind Sivasubramanian, Veerappan Anbazhagan, Jacalin capped silver nanoparticles minimizes the dosage use of the anticancer drug, shikonin derivatives against human chronic myeloid leukemia, *J. Name*., 2013, 00, 1-3
[15]. L. S. B. Upadhyay, N. Verma, Synthesis and characterization of cysteine functionalized silver nanoparticles for biomolecule immobilization, Bioprocess Biosyst. Eng. 37 (2014) 2139-2148.
[16]. Shakeel Ahmed, Saifullah, Mudasir Ahmad, Babu Lal Swami & Saiqa Ikram, Green synthesis of silver nanoparticles using Azadirachta indica aqueous leaf extract,Journal of Radiation Research and Applied Sciences 9(2016)1-7

[17]. Yen, F.L., Wu, T.H., Lin, L.T., Cham, T.M., Lin, C.C.:Naringenin-loaded nanoparticles improve the physicochemical properties and the hepatoprotective effects of naringenin in orally-administered rats with CCl(4)-induced acute liver failure. Pharm Res, 26, 893–902 (2009). https://doi/ 10.1007/s11095-008-9791-0
[18]. Manthey, J.A., Grohmann, K., Guthrie, N.: Biological properties of citrus flavonoids pertaining to cancer and inflammation. Curr. Med. Chem, 8, 135–153 (2001). https://doi/ 10.2174/0929867013373723
[19]. Bugianesi, R., Catasta, G., Spigno, P., A.D'Uva., Maiani, G.:Naringenin from cooked tomato paste is bioavailable in men. J. Nutr 132, 3349–3352 (2002).
[20]. Erlund, I.: Review of the flavonoids quercetin, hesperetin, and naringenin. Dietary sources, bioactivities, bioavailability, and epidemiology. Nutr Res 24, 851–874 (2004). https://doi.org/10.1016/j.nutres.2004.07.005
[21]. Barbinta-Patrascu, N.E., Badea, N., Ungureanu, C., Constantin, M., Pirvu, C., Rau, I.: Silver-based biohybrids ''green'' synthesized from *Chelidoniummajus L.* Opt Mater, 56, 94-96 (2015). https://doi.org/10.1016/j.optmat.2015.10.021
[22]. Sahu, N., Soni, D., Chandrashekhar, B., Satpute, D.B., Saravanadevi, S., Sarangi B.K., et al.: Synthesis of silver nanoparticles using flavonoids: hesperidin, naringin and diosmin, and their antibacterial effects and cytotoxicity. Int Nano Lett, 6, 173–181 (2016). https://doi.org/10.1007/s40089-016-0184-9
[23]. Saptarshi, S.R., Duschl, A., Lopata, A.L.: Interaction of nanoparticles with proteins: relation to bio-reactivity of the nanoparticle. J. Nanobiotechnol, 11, 26 (2013). https://doi.org/10.1186/1477-3155-11-26
[24]. Sahoo, S., Parveen, S., Panda, J.: The present and future of nanotechnology in human health care. NanomedNanotechnolBiol Med 3 20–31 (2007). https://doi.org/10.1016/j.nano.2006.11.008
[25]. Wagner, V., Dullaart, A., Bock, A.K., Zweck, A.: The emerging nanomedicine landscape. Nat Biotechnol, 24, 1211–1217 (2006). https://doi.org/ 10.1038/nbt1006-1211
[26]. Han, G., Ghosh, P., Rotello, V.M.: Functionalized gold nanoparticles for drug delivery. Nanomedicine, 2, 113–123 (2007). https://doi.org/10.2217/17435889.2.1.113
[27]. Guo, S., Huang, L.: Nanoparticles containing insoluble drug for cancer therapy, BiotechnolAdv, 32, 778–788 (2014). https://doi.org/10.1016/j.biotechadv.2013.10.002
[28]. Panyam, J., Labhasetwar, V.: Biodegradable nanoparticles for drug and gene delivery to cells and tissue. Adv. Drug Deliv Rev 55, 329–47 (2003). https://doi.org/10.1016/S0169-409X(02)00228-4
[29]. Huang, S., Qiu, H., Xie, J., Huang, C., Su W., Hu B., et al.: Systematical investigation of in vitro molecular interaction between fluorescent carbon dots and human serum albumin. RSC Adv, 6, 44531–44542 (2016). https://doi.org/10.1039/C6RA01386D
[30]. Alia, M.S., Altaf, M., Hamad, A.,Al-Lohedana, H.A.: Green synthesis of biogenic silver nanoparticles using *Solanumtuberosum* extract and their interaction with human serum albumin: Evidence of "corona" formation through a multi-spectroscopic and molecular docking analysis. J. Photochem. Photobiol, B: Biology, 173, 108–119 (2017). https://doi.org/10.1016/j.jphotobiol.2017.05.015
[31]. Zhu, W., Wang, Q., Dan Su, D.: Study on the Interaction between cadmium sulphide nanoparticles and proteins by resonance Rayleigh scattering spectra. J.Chem, 2013, 1-7(2013). http://dx.doi.org/10.1155/2013/583148
[32]. Prasanth, S., Sudarsanakumar, C.: Elucidating the interaction of L-cysteine-capped selenium nanoparticles and human serum albumin: spectroscopic and thermodynamic analysis. New J. Chem, 41, 9521-9530(2017). http://dx.doi.org/10.1039/C7NJ00477J
[33]. Sen, T., Mandal, S., Haldar, S., Chattopadhyay, K., Patra, A.: Interaction of gold nanoparticle with human serum albumin (HSA) Protein Using Surface Energy Transfer. J. Phys. Chem. C 115, 24037–24044 (2011). http://dx.doi.org/10.1021/jp207374g
[34]. 34.Khan, M.J.,Maskat, M.Y.: Interaction of titanium dioxide nanoparticle with human serum albumin: a spectroscopic approach, IJPPS, 6, 43-46 (2014).
[35]. Bhogale, A., Patel, N., Mariam, J., Dongre, P.M., Miotello, A., Kothari, D.C.: Study of interaction of ZnO nanoparticles with human serum albumin usding fluorescence spectroscpopy. AIP Conf. Proc, 1512, 130-131 (2013).
[36]. Carter, D.C., Ho, J.X.: Structure of serum albumin. Adv. Protein Chem. 45 153-203 (1994).
[37]. Zunszain, P.A., Ghuman, J., McDonagh, A.F., Curry, S.: Crystallographic analysis of human serum albumin complexed with 4Z, 15E-Bilirubin-Ixα. J Mol. Biol.381, 394–406 (2008). https://doi.org/10.1016/j.jmb.2008.06.016
[38]. Park, K.K., Park, W., Hamilton, A.D.: Novel 7-(Dimethylamino) fluorene-based fluorescent probes and their binding to human serum albumin. Org. Biomol. Chem, 7, 4225–4232 (2009). https://doi.org/10.1039/B911605B
[39]. Yang, F., Zhang, Y.,Liang, H.: Interactive association of drugs binding to human serum albumin. Int. J. Mol. Sci, 15, 3580–3595 (2014). https://doi.org/10.3390/ijms15033580
[40]. Ghuman, J., Zunszain, P.A., Pepitas I., Bhattacharyja, A.A., Otagiri, M., Curry, S.:Structural basis of the drug-binding specificity of human serum albumin. J. Mol. Biol, 353, 38-52 (2005). https://doi.org/10.1016/j.jmb.2005.07.075
[41]. Simard, J.R., Zunszain, P.A., Hamilton, J.A., Curry, S.:Location of high and low affinity fatty acid binding sites on human serum albumin revealed by NMR drug-competition analysis. J. Mol. Biol, 361, 336-351 (2006). https://doi.org/10.1016/j.jmb.2006.06.028
[42]. Engelborghs, Y.: The analysis of time resolved protein fluorescence in multi-tryptophan proteins. SpectrochimActa A, 57, 2255–2270 (2001). https://doi.org/10.1016/S1386-1425(01)00485-1

[43]. Velmurugan, P., Sivakumar, S., Young-Chae, S., Seong-Ho, J., Pyoung-In, Y., et al.: Synthesis and characterization comparison of peanut shell extract silver nanoparticles with commercial silver nanoparticles and their antifungal activity. Ind. Eng. Chem. Res,31, 51–54 (2015). https://doi.org/10.1016/j.jiec.2015.06.031
[44]. P.Jegadeeswaran, Rajeshwari shivaraj , R.Venckatesh.: Green synthesis of silver nanoparticles from extract of padina tetrastromatica leaf: Digest Journal of Nanomaterials and Biostructures 7, 991 – 998(2012)
[45]. Raj, D.R., Sudarsanakumar, C.:Surface plasmon resonance based fiber optic sensor for the detection of cysteine using diosmin capped silver nanoparticles.Sens Actuators A-Phys, 253, 41-48(2017). https://doi.org/10.1016/j.sna.2016.11.019
[46]. Srikar, S.K., Giri, D.D., Pal, D.B., Mishra, P.K., Upadhyay, S.N.: Green synthesis of silver nanoparticles: A review. Green and Sustainable Chemistry, 6, 34-56 (2016). https://doi.org/10.4236/gsc.2016.61004
[47]. Prasanth, S., Varughese, M., Joseph, N., Mathew, P., Manojkumar, T.K., Sudarsanakumar, C.: FTIR: Crystal Structure, FT-IR, FT-Raman, 1HNMR and Computational study of Ethyl2-{[(Z)3-(4-chlorophenyl)-3-hydroxy-2-propene-1-thione]amino} acetate. J Mol. Struct, 1081, 366-374 (2015). https://doi.org/10.1016/j.molstruc.2014.10.037
[48]. Li, L., Zhang, Q., Ding, Y., Cai, X., Gu, S., Cao, Z.: Analytical methods application of L-cysteine capped core-shell CdTe/ZnS nanoparticles as a fluorescence Probe for cephalexin. Anal. Methods, 6, 2715–2721 (2014). https://doi.org/10.1039/C4AY00094C
[49]. Shang, L., Wang, Y., Jiang, J., Dong, S.:pH-Dependent Protein conformational changes in albumin:gold nanoparticle bioconjugates: A spectroscopic study. Langmuir 232714–2721 (2007). https://doi.org/10.1021/la062064e
[50]. Sen, S., Konar, S., Das, B., Pathak, A., Dhara, S., Dasgupta, S., et al.: Inhibition of fibrillation of human serum albumin through interaction with chitosan-based biocompatible silver nanoparticles. RSC Adv 6 43104–43115 (2016). https://doi.org/10.1039/C6RA05129D
[51]. Rastegari, B., Karbalaei-heidari, H.R., Yousefi, R., Zeinali, S.: Interaction of prodigiosin with HSA and B-Lg: spectroscopic and molecular docking studies. Bioorg. Med. Chem, 24, 1504–1512 (2016). https://doi.org/10.1016/j.bmc.2016.02.020
[52]. Prasanth, S., Raj, D.R., Vineeshkumar, T.V., Thomas, R.K., Sudarsanakumar, C.: Exploring the interaction of L-cysteine capped CuS nanoparticles with bovine serum albumin (BSA): a spectroscopic study. RSC Adv, 6, 58288-58295 (2016).https://doi.org/ 10.1039/c6ra03583c
[53]. Pragash, R., Jose, G., Unnikrishnan, N.V.,Sudarsanakumar, C.: Energy transfer and thermal studies of Pr3+ doped cerium oxalate crystals. Bull. Mater. Sci, 34, 955–961 (2011).
[54]. Bhogale, A., Patel, N., Mariam, J., Dongre, P.M., Miotello, A., Kothari, D.C.: Comprehensive studies on the interaction of copper nanoparticles with bovine serum albumin using various spectroscopies. Colloids Surf B: Biointerfaces113 276–284 (2014). https://doi.org/10.1016/j.colsurfb.2013.09.02
[55]. Sen, T., Sadhu, S., Patra, A.: Surface energy transfer from rhodamine 6 G to gold nanoparticles: A spectroscopic ruler. Appl. Phys. Lett, 91, 043104 (2007). https://doi.org/10.1063/1.2762283
[56]. Limo, M.J., Perry C.C.: Thermodynamic study of interactions between ZnO and ZnO binding peptides using isothermal titration calorimetry. Langmuir, 31, 6814–6822 (2015). https://doi.org/10.1021/acs.langmuir.5b01347
[57]. Chakraborti, S., Joshi, P., Chakravarty, D., Shanker, V., Ansari, Z.A., Singh, S.P., et al.: Interaction of Polyethyleneimine-Functionalized ZnO nanoparticles with bovine serum albumin, Langmuir, 2811142–11152 (2012). https://doi.org/10.1021/la3007603
[58]. Das, K., Kamla, K., Rajan, R., Bohidar, H.B.: Size dependent CdSe quantum dot-lysozyme interaction and effect on enzymatic activity. RSC Adv,6, 46744-46754 (2016). https://doi.org/10.1039/C6RA07368A
[59]. Li Shanghao., ZhiliPeng., Roger, M., Leblanc, A.: Simple method to determine protein concentration in the protein-nanoparticle conjugates aqueous solution using circular dichroism spectroscopy, Anal. Chem, 87, 6455–6459 (2015).
[60]. Hou, H.N., Qi, Z.D., OuYang, Y.W., Liao, F.L., Zhang, Y., Liu, Y.: Studies on interaction between Vitamin B12 and human serum albumin. J Pharm Biomed. Anal, 47, 134–139 (2008). https://doi.org/10.1016/j.jpba.2007.12.029
[61]. Jash, C., Kumar, G.S.: Binding of Alkaloids Berberine, Palmatine and coralyne to lysozyme: A combined structural and thermodynamic study. RSC Adv 4, 12514−12525 (2014). https://doi.org/10.1039/C3RA46053C
[62]. Jash, C., Payghan, P.V., Ghoshal, N., Kumar, G.S.: Binding of the Iminium and alkanolamine forms of sanguinarine to lysozyme: spectroscopic analysis, thermodynamics, and molecular modeling studies. J. Phys. Chem. B, 118, 13077-13091 (2014). https://doi.org/10.1039/10.1021/jp5068704

